Catalysis Science & Technology

PAPER

View Article Online
View Journal | View Issue

Cite this: *Catal. Sci. Technol.*, 2016, **6**, 3900

Re-designing the substrate binding pocket of laccase for enhanced oxidation of sinapic acid†

I. Pardo,[a] G. Santiago,[b] P. Gentili,[c] F. Lucas,*[bd] E. Monza,[b] F. J. Medrano,[a] C. Galli,[c] A. T. Martínez,[a] V. Guallar[be] and S. Camarero*[a]

Received 9th October 2015,
Accepted 28th December 2015

DOI: 10.1039/c5cy01725d

www.rsc.org/catalysis

Iterative saturation mutagenesis was performed over six residues delimiting the substrate binding pocket of a high redox potential chimeric laccase with the aim of enhancing its activity over sinapic acid, a lignin-related phenol of industrial interest. In total, more than 15 000 clones were screened and two selected variants, together with the parent-type laccase, were purified and characterized. The new variants presented shifted pH activity profiles and enhanced turnover rates on sinapic acid and its methyl ester, whereas the oxidation of related phenols was not significantly enhanced. Neither the enzyme's redox potential nor the mechanism of the reaction was affected. Quantum mechanics and molecular dynamics calculations were done to rationalize the effect of the selected mutations, revealing the critical role of the residues of the enzyme pocket to provide the precise binding of the substrate that enables an efficient electron transfer to the T1 copper. The results presented highlight the power of combining directed evolution and computational approaches to give novel solutions in enzyme engineering and to understand the mechanistic reasons behind them, offering new insights for further rational design towards specific targets.

Introduction

Laccases are multi-copper oxidases capable of oxidizing a wide range of compounds, especially substituted phenols and aromatic amines, coupled with the reduction of molecular oxygen to water. Some laccases secreted by white-rot fungi involved in lignin degradation (typically belonging to the order Polyporales) stand out for their high redox potential at the T1 copper site (E^0 ~0.8 V) compared to laccases from other fungi, plants or bacteria (from 0.4 to 0.7 V). Moreover, the use of redox mediators, which are small molecules that can act as diffusible electron shuttles between the substrate and laccase, can further extend the oxidative capabilities of these enzymes. In previous studies we described the ability of certain phenolic compounds related to lignin to act as laccase mediators.[1,2] The combined application of laccase and these natural mediators might be a key factor for the integrated use of plant biomass in lignocellulosic biorefineries for the sustainable production of chemicals, materials and fuels.[3,4]

The potential of laccases as industrial biocatalysts has led to numerous efforts to engineer these enzymes with the aim of enhancing their activity and/or stability for industrial application.[5] In this sense, directed evolution has proven to be a powerful tool to obtain laccases *a la carte*. In a previous work we described the construction of chimeric laccases by random DNA shuffling of two high redox potential laccases (HRPLs) from basidiomycetes PM1 and *Pycnoporus cinnabarinus* expressed in *Saccharomyces cerevisiae*.[6–8] The new laccases presented improved properties with respect to both parent types, including better substrate affinities and increased stability towards temperature and pH.

Using one chimeric laccase (3A4) with increased affinity towards phenols as a scaffold, we aim here to enhance its activity towards sinapic acid (SA). This *p*-hydroxycinnamic acid is of biotechnological interest for a) its ability to act as a laccase mediator; b) the biological activity (as an antioxidant, antimicrobial, immunomodulatory, antitumoral or UV-B screening agent) of SA itself, its esters or other derivatives;[2,9–12] and c) the role of sinapate dehydrodimers or heterodimers (with ferulate) in cross-linking polysaccharides in grass cell walls. Indeed, *p*-hydroxycinnamic acids are one of the main inhibitory phenolic compounds released during the physico-chemical pretreatment of lignocellulose for ethanol production. Detoxification of wheat straw slurries by laccase, after the enzymatic hydrolysis or during the

[a] *Centro de Investigaciones Biológicas, CSIC, Ramiro de Maeztu 9, 28040 Madrid, Spain. E-mail: susanacam@cib.csic.es*
[b] *Joint BSC-CRG-IRB Research Program in Computational Biology, Barcelona Supercomputing Center, c/Jordi Girona 29, 08034 Barcelona, Spain. E-mail: fatima.lucas@bsc.es*
[c] *Dipartimento di Chimica, Università "La Sapienza" and IMC-CNR Sezione Meccanismi di Reazione, P.le A. Moro 5, 00185 Rome, Italy*
[d] *Anaxomics Biotech, Balmes 89, E-08008 Barcelona, Spain*
[e] *ICREA, Passeig Lluís Companys 23, 08010 Barcelona, Spain*

† Electronic supplementary information (ESI) available. See DOI: 10.1039/c5cy01725d

simultaneous saccharification and fermentation, has been described to enhance yeast fermentation performance and raise the final ethanol yields,[13,14] allowing working also at higher substrate consistencies.[15]

To this end, we describe here the re-design of the laccase's substrate binding pocket by iterative saturation mutagenesis (ISM)[16] of six residues limiting the cavity. This is the first time that the systematic exploration of all possible amino acid substitutions and their combinations is attempted in laccases as compared to previous works.[17–19] At the same time we address the biochemical and mechanistic characterization of two engineered laccase variants selected for their increased activity towards SA, together with the computational simulations performed to rationalize the effect of the inserted mutations.

Experimental section

Construction of mutant libraries

Sequences of laccases from basidiomycetes of the order Polyporales were retrieved from UniProt KB, filtering for a minimum length of 450 amino acids and clustering identical sequences. Selected sequences were aligned using T-Coffee[20] and sequence logos were generated with the WebLogo 3[21] server. The most variable residues delimiting the substrate binding pocket (six in total) were selected for mutagenesis. Mutant libraries were obtained using IVOE,[22] using the pJRoC30 plasmid containing the 3A4 coding sequence fused to an evolved alpha-factor pre-proleader as template.[8] Complementary mutagenic primers were designed so that degenerate codons (NNK, where N = A/C/G/T and K = G/T) were flanked by ~20 bp (Table S1†). For each mutagenesis site two PCRs were performed: one with RMLN and the reverse mutagenic primer, and another with RMLC and the forward mutagenic primer. RMLN and RMLC primers anneal with pJRoC30 plasmid, flanking the α-3A4 CDS. The PCR conditions, product purification and *in vivo* cloning in competent *S. cerevisiae* BJ5465 cells have been described previously.[8]

Screening of mutant libraries

For each mutant library, at least 3066 clones were analyzed in order to obtain 95% library coverage (two positions with NNK degeneracy). Culture media for cell growth and laccase expression in 96-well plates, and the general procedure for library screening and the two re-screenings were described previously.[7,8] In this work, libraries were screened for activity towards 250 μM SA (at 512 nm) in 100 mM acetate buffer, pH 5.[7,23] A thermostability screening assay was also performed with some selected clones.[24]

Production and purification of mutated laccases

Individual colonies of selected clones were grown in minimal medium (6.7 g L^{-1} YNB, 1.92 g L^{-1} Drop-Out Media Supplements without uracil, 2% raffinose and 25 mg L^{-1} chloramphenicol) for 48 h at 30 °C and 220 rpm. Aliquots of these cultures were used to inoculate 30 mL of minimal medium in 250 mL flasks to an OD_{600} = 0.25, which were incubated until an OD_{600} = 1 was reached. Then, cells were diluted tenfold to a final volume of 300 mL with laccase expression minimal medium (6.7 g L^{-1} YNB, 1.92 g L^{-1} Drop-Out Media Supplements without uracil, 2% galactose, 67 mM phosphate buffer, pH 6, 1 mM $CuSO_4$, and 25 mg L^{-1} chloramphenicol) in 1 L flasks. Cultures were grown at 30 °C and 220 rpm until maximum laccase activity was reached (3–4 days). Standard laccase activity assay consisted in measuring the oxidation of 3 mM 2,2′-azino-bis(3-ethylbenzothiazoline-6-sulfonic acid) (ABTS) in 100 mM acetate buffer (pH 5) in a spectrophotometer ($ABTS^{+}\cdot$, ε_{418} = 36 000 M^{-1} cm^{-1}), defining one unit of laccase as the amount of enzyme needed to transform 1 μmol ABTS per minute.

Cultures were centrifuged at 10 000*g* for 15 min at 4 °C, and supernatants were consecutively filtered through 0.8 and 0.45 μm pore-size membranes. Then, crude extracts were concentrated by ultra-filtration through 10 000 MWCO membranes and dialyzed against 20 mM Tris-HCl buffer, pH 7. Laccases were purified by HPLC (AKTA purifier, GE Healthcare) in two anion-exchange steps and one molecular exclusion step: first, using a HiPrep Q FF 16/10 column and a 100 mL gradient of 0–40% elution buffer (20 mM Tris-HCl + 1 M NaCl, pH 7); second, using a Mono Q HR 5/5 column and a 30 mL gradient of 0–25% elution buffer; and finally using a HiLoad 16/600 Superdex 75 pg column and 20 mM Tris-HCl + 150 mM NaCl, pH 7 (all columns from GE Healthcare). Fractions containing laccase activity were pooled, dialyzed and concentrated between each chromatographic step.

Biochemical characterization of laccase variants

Microplate assays to determine T_{50} (10 min), pH activity profiles, and kinetic constants of purified laccase variants were described previously.[7] Kinetic constants for SA (ε_{312} = 17 600 M^{-1} cm^{-1}), methyl sinapate (MS, ε_{320} = 18 855 M^{-1} cm^{-1}) and 2,6-dimethoxyphenol (DMP, product ε_{469} = 27 500 M^{-1} cm^{-1}, referred to as DMP concentration) were determined in 96-well plates, using UV-transparent microplates for SA and MS (UV-Star, Greiner Bio-One). Kinetic constants for dehydrodisinapic acid dilactone (DAD, product ε_{530} = 17 000 M^{-1} cm^{-1}, referred to as DAD concentration) were determined in a spectrophotometer using 1 cm path quartz cuvettes. In the case of syringic acid (SyA, ε_{260} = 9035 M^{-1} cm^{-1}) and methyl syringate (MSy, ε_{275} = 11 660 M^{-1} cm^{-1}), reactions were carried out in 0.1 cm path quartz cuvettes. Due to the high initial absorbance of MSy, reactions for higher concentrations (mM range) were followed discontinuously, taking aliquots at different time-points and diluting 10-fold prior to measuring A_{275}. The chemical structure of phenolic compounds for which kinetic constants were obtained is shown in Fig. S1.†

Competition reactions with *p*-X-substituted phenols were carried out as described previously[25] with slight

modifications: 2 or 5 units of the different variants were added to a 600 μL mixture of O_2-saturated 100 mM citrate buffer (pH 5) and dioxane (v:v ratio 2:1) containing 6 μmol of each phenolic substrate. Reactions proceeded at room temperature with stirring and under O_2 atmosphere. After the addition of 4-methoxyacetophenone as internal standard and extraction with ethyl acetate, the consumption of substrates at end-point was determined with an Agilent 6850 Series II GC equipped with a methyl silicone capillary column. Hammett plots were obtained by representing relative reaction constants $\log(k_X/k_H)$ *versus* σ^+ for the different *p*-X-substituted phenols and fitting to a straight line.

Redox potentials of the different variants were determined by the poised potential method using the redox couple $Fe(dipyridyl)_2Cl_2/Fe(dipyridyl)_2Cl_3$ in 8 mM MES buffer (pH 5.3).[25,26] Oxidation of $Fe(dipyridyl)_2Cl_2$ at each titration point was followed by the decrease in absorbance at 522 nm (ε_{522} = 5974 M^{-1} cm^{-1}) until equilibrium was reached. The concentration of reduced laccase at equilibrium was considered to be 1/4 of the oxidized $Fe(dipyridyl)_2Cl_2$ concentration.

Marcus plots were obtained by representing $\ln(k_X/k_H)$ *versus* $\Delta G°$, calculated from the difference in redox potentials between the laccase and the different *p*-X-substituted phenols. Reorganization energies for electron transfer were calculated by fitting data to the following equation:[25] $\ln(k_X/k_H) = \ln(k_BT/h) - \ln k_H - \Delta G^{\#}/RT$, where $\Delta G^{\#} = (\lambda/4)(1+\Delta G°/\lambda)^2$.

Synthesis of DAD

SA was dissolved in 80 mL of acetonitrile (27.5 mM concentration), and then 80 mL of a 27.5 mM aqueous solution of $CuSO_4$ was added. The mixture was stirred for 6 h at room temperature and evaporated to dryness at 40 °C under reduced pressure. The solid residue was redissolved in water and extracted with ethyl acetate. The organic layers were washed with brine, dried over anhydrous Na_2SO_4, and concentrated under vacuum to give the SA lactone dimer (308 mg, 0.69 mmol).[27] Crystallization from aqueous acetone yielded dilactone as yellow prisms (m.p. 212–214 °C, lit 208°).[28,29] The structure was confirmed by NMR in acetone-d_6. ^{1}H NMR spectrum (300 MHz,) δ (ppm): 7.60 (brs, 1H, OH), 6.74 (s, 4H), 5.76 (s, 2H), 4.12 (s, 2H) and 3.84 (s, 12H). ^{13}C NMR spectrum (75 MHz) δ (ppm): 176.8, 149.7, 138.1, 130.6, 105.0, 84.2, 57.5 and 49.8.

System setup for computational simulations

The initial structure was taken from the coordinates of PM1L (PDB 5ANH), which shares 98% sequence identity with the chimeric variant 3A4. The 3A4 model contains a single mutation in the substrate binding pocket regarding PM1L (V162A), selected during the directed evolution of PM1L.[6] The C14F12 model additionally introduces F392N, while the CA32F1 model includes mutations V162R, T164E and F392N. In the first two proteins mutations were modeled with Maestro (version 10.0, Schrodinger, LLC, New York, NY, 2014), allowing for the modified amino acid and its neighbors (5 Å distance) to relax with IMPACT (version 6.5, Schrodinger, LLC, New York, NY, 2014). In the case of CA32F1, however, the introduction of a large side chain in position 162 (V to R) required further attention, and 20 ns of molecular dynamics (MD) simulation with DESMOND[30] was performed to assure the model's stability (see the ESI†).

The protonation state of titratable residues was estimated with the Protein Preparation Wizard (PROPKA) and the H++ server (http://biophysics.cs.vt.edu/H++) followed by visible inspection.[31–33] At pH 5 (in which most of the experiments were performed) histidines 55, 71, 91, 133, 153 and 401 were established to be fully protonated (positively charged); 66, 394 and 455 were ε-protonated; and all others were δ-protonated. Aspartic acids 50, 77, 101, 453 and 467 and glutamic acids 308 and 470 were also found to be protonated at pH 5. Further experiments were conducted at pH 3 and predicted pK_a values showed no changes in protonation states for both 3A4 and C14F12 (in particular in the binding pocket, where D205 is found to have a pK_a of 1.2 and 1.8, respectively). In CA32F1, however, D205 has an increased pK_a of 3.8 and for this reason extra simulations for this system were also performed with protonated D205.

With an experimentally determined pK_a of 4.9,[34] SA is expected to have the protonated (SAH) and deprotonated (SA^-) species in equilibrium at pH 5, and so all simulations have been performed with both models. Structures for SA, DAD and MS were fully optimized with Jaguar[35] in an implicit solvent and electrostatic potential charges were computed with the density functional M06 at the 6-31G* level of theory. From these, ligand parameters were extracted for the classic simulations.

PELE sampling

To sample the binding modes of the three computationally studied substrates (SA, DAD and MS) in the chimeric proteins, we have used the Protein Energy Landscape Exploration (PELE) software.[36] PELE is a Monte Carlo algorithm composed of a sequence of perturbation, relaxation, and a Metropolis acceptance test. In the first step, the ligand is subjected to random rotations and translations while the protein is perturbed based on the anisotropic network model (ANM).[37] For ligand perturbation the maximum allowed translation was 2.2 Å and the maximum rotation was 20°. For the protein perturbation all atoms are displaced (a maximum of 0.5 Å) by moving α-carbons to follow a random linear combination of the 6 lowest eigenvectors obtained in the ANM model. The relaxation step includes the repositioning of all amino acid side chains within 6 Å of the ligand and the 5 side chains with the highest energy increase along the previous ANM step. The relaxation stage ends with a truncated Newton minimization using the OPLS all-atom force field and an implicit surface-generalized Born continuum solvent.[38,39] New proposed minima are then accepted or rejected based on a Metropolis test. Substrate binding plots contain

all accepted conformations for three 48 h simulations using 40 processors.

Quantum mechanics/molecular mechanics (QM/MM)

After applying an energy filter, randomly selected structures from PELE simulations were further optimized through five cycles of geometry optimization using Qsite,[40] and the atomic Mulliken spin density of the substrate was computed.[41] The protein is modelled classically using the OPLS force field while the substrate, the T1 copper atom, and residues H394, C450, H455, I452 and F460 are included in the quantum region. The density functional method employed was the M06-L functional, with the LANL2DZ effective core basis set for the copper atom and the 6-31G* for all other atoms.[42,43]

Results and discussion

Construction and screening of mutant libraries

Inspection of the molecular model for the parent 3A4 laccase revealed that the substrate binding pocket was delimited by amino acids in positions 162–164, 263, 264, 331, 336 and 390–392. In order to select the target residues for mutagenesis, we performed a multiple sequence alignment of laccases from fungi of the order Polyporales (including *P. cinnabarinus* and basidiomycete PM1) (Fig. 1). Residues in positions 162, 164, 263, 264, 390 and 392 (according to 3A4 laccase numbering) were the most variable and, therefore, were chosen for randomization. As simultaneous combinatorial saturation mutagenesis (CSM) of the six sites would imply screening more than 10^9 clones for 95% library coverage, we used the ISM approach in order to diminish the screening effort.[16] In our case, we defined three regions, each comprising two target residues for mutagenesis: region A, for residues 162 and 164; region B, for residues 263 and 264; and region C, for residues 390 and 392. Individual libraries were constructed for each region and in this way the number of clones to be screened for 95% coverage was reduced to 3066 per library.

The mutant libraries were screened with SA at pH 5. This pH is described as the working pH for the enzymatic saccharification and yeast fermentation of prehydrolyzates from wheat straw biomass to produce ethanol.[44] Owing to the common acidic pH of laccases, the availability of recombinant enzymes with more neutral optimum pH is of interest for biomass conversion processes. Activity landscapes of first generation mutant libraries A, B and C revealed different plasticity among regions, *i.e.*, the admission of amino acidic variability in the selected positions (Fig. 2A). Region B was the least flexible of the three studied, with 83% of clones presenting less than 5% activity with respect to the parent laccase, followed by region A (48%) and region C (29%). The latter presented a high proportion of clones with better activity than the parent type. A first re-screening was performed to rule out false positives, and plasmids from selected clones from each library were extracted and sequenced (Table S2†). In the case of library A, the selected clones mutated A162 for polar residues. Notably, several included basic amino acids, even though the sequence alignment of laccases showed conserved hydrophobic residues in this position (mostly phenylalanine). All five clones from library B that were sequenced maintained N263, indicating its essential role for the activity of these laccase variants (even though this position is quite variable among polyporus laccases). Finally, mutations in library C were the most variable, although the most frequent were the substitution F392N and the conservation of P390.

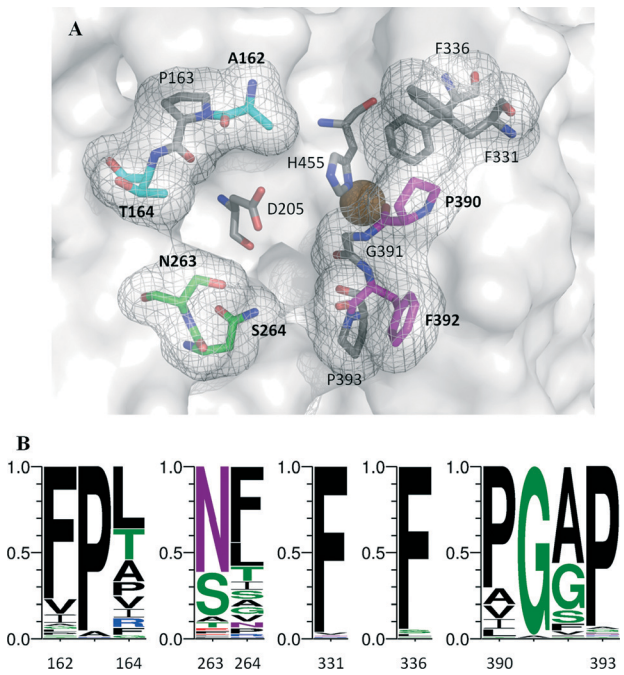

Fig. 1 (A) Residues delimiting the substrate binding pocket of 3A4 laccase. Residues selected for mutagenesis are shown in cyan (region A), green (region B) and magenta (region C). Conserved residues His 455 and Asp 205, respectively involved in electron and proton transfer, are also shown. (B) Sequence logo for residues delimiting the substrate binding pocket in laccases of Polyporales. Heights indicate relative frequencies. Hydrophobic residues are shown in black, polar residues in green, acid residues in red, basic residues in blue and neutral residues in purple.

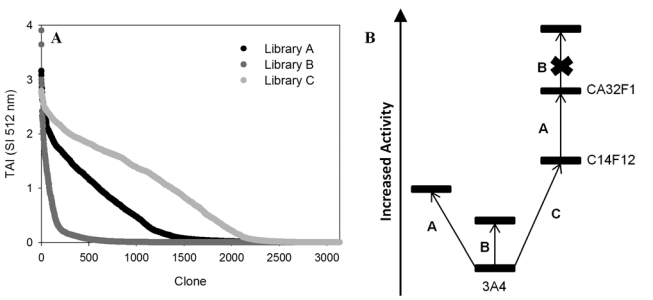

Fig. 2 (A) Activity landscapes for mutant libraries A (black), B (dark gray) and C (light gray). (B) Representation of the ISM pathway followed in this work.

Next, a second re-screening, in which plasmids were re-transformed in yeast, was performed simultaneously for selected mutants from the three libraries. In general, total activity increase (TAI) values decreased in the order C > A > B, so the ISM pathway was defined as shown in Fig. 2B: the winner from library C would be used as a scaffold for the mutagenesis of region A (library CA), and the winner of this library would then be used as a scaffold for the mutagenesis of region B (library CAB). In order to select the clone from library C to be used as the parent for the next round of mutagenesis, ten clones showing the highest TAI values (2.5- to 4-fold higher than that of 3A4) were further subjected to a thermostability assay to discard any destabilizing mutations (Fig. S2†). In general, we observed that clones that maintained P390 were the most stable. Hence, C14F12 mutant (F392N), with around 4-fold TAI and increased stability with respect to the 3A4 parent type, was selected as the winner.

The activity landscape of library CA was similar to that observed for library A, although apparently the number of clones that retained parent activity was somewhat lower (Fig. S3A†). Sequencing of selected clones revealed a possible epistatic relationship between mutations in region A and mutation F392N. This substitution seemed to favor the appearance of an acid–basic residue pair in positions 162 and 164 (Table S2†), a bias that was not observed in library A. It is worth noting that available structures of fungal laccases co-crystallized with different substrates,[45,46] and site-directed mutagenesis studies[17,47] suggest that non-polar residues in these positions are essential for substrate–enzyme recognition, establishing hydrophobic interactions with the substrate's aromatic ring. This apparent contradiction could be explained by the increased polarity of the phenolic ring of SA due to the presence of two methoxyl groups, which could interact with the polar residues in positions 162 and 164.

As in the first generation, a thermostability screening was performed for selected clones from library CA, but no significant changes in stability were found. Therefore, the most active mutant CA32F1 (A162R/T164E/F392N) was selected as the parent type for the third generation. In accordance with what was observed for libraries A and CA, the activity landscape for library CAB was similar to that of library B, although maximum TAI values were not as high (Fig. S3B†). Moreover, after screening over 5000 clones, DNA sequencing revealed that all clones selected held no new mutations.

Biochemical characterization of selected ISM variants

Parent laccase 3A4 and variants C14F12 and CA32F1 were produced and purified to homogeneity for their characterization. While 3A4 and C14F12 presented T_{50} values of ~70 °C, it decreased to 67 °C for CA32F1. ISM variants presented similar pH activity profiles for SA oxidation, more neutral compared to that of the parent type (Fig. 3): the optimum pH was 4 for all laccases, but the second best value (relative activity >80%) was obtained at pH 3 for 3A4 and at pH 5 for both C14F12 and CA32F1. This is a consequence of the selective pressure applied during library screening, performed at pH 5, as has been described in other laccase-directed evolution studies.[7,48–50] Concerning reaction kinetics for SA at pH 5 (Table 1), ISM variants presented increased k_{cat} values, around 1.6-fold with respect to the parent type. Although these increments are not as high as desirable, it should be taken into account that SA is a natural substrate of fungal laccase and, hence, an enhancement of severalfold in k_{cat} is difficult to achieve. For instance, during the active site redesign of a small bacterial laccase towards 2,6-dimethoxyphenol, severalfold improvements were attained by punctual mutations, but the wild-type activity on this substrate was extremely low (k_{cat} 0.87 s^{-1}).[18] Concerning K_m, C14F12 laccase presented a 2-fold increase with respect to parent 3A4, whereas affinity was somewhat recovered in CA32F1. In all, catalytic efficiencies for SA at pH 5 are not significantly affected in the new variants. Nevertheless, it should be mentioned that from an industrial point of view, increasing the turnover rates is the aim, independently of the changes obtained in K_m, since substrate concentration does not represent a limiting factor in industrial enzymatic transformations (where high amounts of substrate are generally applied). It is also worth noting that despite the shifted pH activity profiles, CA32F1 still presents a higher turnover rate (and catalytic efficiency) towards SA than the 3A4 parent type at pH 3.

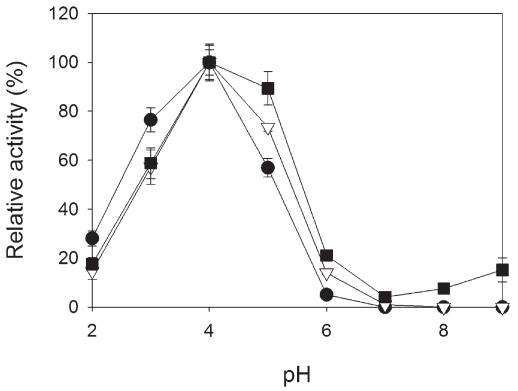

Fig. 3 pH activity profiles with SA for laccase variants 3A4 (circles), C14F12 (triangles) and CA32F1 (squares). Means were obtained from triplicates; error bars represent standard deviations.

Table 1 Kinetic constants for the oxidation of SA and DAD by the parent-type laccase 3A4 and the ISM variants (C14F12 and CA32F1). Reactions at pH 5 were performed in 100 mM acetate buffer, while reactions at pH 3 were performed in 100 mM tartrate buffer

Substrate		3A4	C14F12	CA32F1
SA (pH 5)	k_{cat} (s^{-1})	156 ± 3	251 ± 4	257 ± 3
	K_m (μM)	7.0 ± 0.7	14.2 ± 0.7	9.9 ± 0.5
	k_{cat}/K_m	22 ± 3	17.7 ± 1.1	26 ± 2
SA (pH 3)	k_{cat} (s^{-1})	313 ± 8	338 ± 3	429 ± 9
	K_m (μM)	92 ± 5	137 ± 13	80 ± 4
	k_{cat}/K_m	3.4 ± 0.3	2.5 ± 0.3	5.3 ± 0.4
DAD (pH 5)	k_{cat} (s^{-1})	68 ± 1	68 ± 3	73 ± 3
	K_m (μM)	21.6 ± 1.3	59 ± 7	66 ± 9
	k_{cat}/K_m	3.2 ± 0.2	1.2 ± 0.2	1.1 ± 0.2

In the HTS assay used for the screening of mutant libraries, the oxidation of SA was followed by the development of a pinkish color (λ_{max} = 512 nm).[23] This colored product is a result of the oxidation of DAD, a phenolic dimeric compound formed from the β–β′ coupling of two phenoxyl radicals of SA that is also a substrate for laccase (Scheme S1†).[47,51] DAD was synthesized and the corresponding kinetic constants for its oxidation by the three laccase variants were obtained to verify whether TAI values observed in the library screenings were due to enhanced activity over SA alone or also to a better oxidation of DAD. Surprisingly, k_{cat} values were not enhanced, and affinity towards DAD was significantly worse for the ISM variants.

Hammett and Marcus correlations

In order to ascertain whether mutations in ISM variants C14F12 and CA32F1 affected the reaction mechanism, Hammett and Marcus plots were obtained for the three laccases. Competition reactions at pH 5 with different *p*-X-substituted phenols (*p*-methoxyphenol, *p*-methylphenol, *p*-phenylphenol, *p*-chlorophenol and phenol) were carried out and $\log(k_X/k_H)$ values were plotted against σ^+ values for each substrate (Fig. S4A–C). Calculated ρ-values for the three laccases were all around −2, indicating that all three laccase variants are similarly dependent on the nature of the *p*-X-substituent group (Table 2). These values are slightly lower than those obtained for other HRPLs from *Trametes villosa* and *Trametes versicolor*.[25,52] Redox potentials for the three laccases were also obtained, but no significant differences were found. The same occurred for total reorganization energies (λ) for electron transfer calculated according to the Marcus equation (Fig. S4D and E†), with values ranging from 45 to 47 kcal mol^{-1} (Table 2), similar to those described for *T. villosa* and *T. versicolor* laccases.[25,52] Similar to these two laccases, these results suggest that 3A4 laccase and ISM variants oxidize phenols by an asynchronous concerted electron–proton transfer mechanism, where the electron transfer to the T1 copper site leads to the formation of a fleeting radical cation reactive intermediate (in agreement with the observed negative ρ-values) and the concomitant proton transfer to the D205 residue leads to a phenoxyl radical product. This feature is appropriately described as an unbalanced transition state, according to Muller (Scheme 1).[53] In all, these results suggest that the selected mutations do not affect the mechanism of the reaction, and thus the increased turnover rates observed in the ISM laccase variants are caused by other factors.

Table 2 Redox potentials (V *vs.* NHE), ρ-values for Hammett plots and reorganization energies (kcal mol^{-1}) for Marcus plots calculated at pH 5 for 3A4 laccase and ISM variants (C14F12 and CA32F1)

Laccase	E^0	ρ (Hammett)	λ (Marcus)
3A4	0.7887 ± 0.0004	−1.9 ± 0.3	44.6 ± 0.3
C14F12	0.783 ± 0.002	−2.1 ± 0.2	47.4 ± 0.4
CA32F1	0.7752 ± 0.0006	−2.2 ± 0.1	45.6 ± 0.5

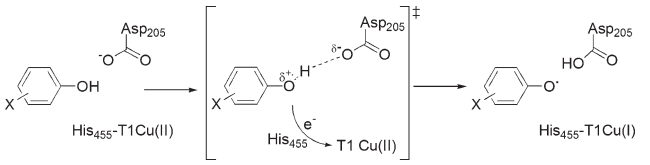

Scheme 1 Concerted electron proton transfer mechanism for the oxidation of phenols by 3A4 laccase and ISM variants.

Computational analysis of substrate binding and oxidation

To rationalize the effect of mutations on substrate oxidation, molecular simulations were performed.[54] The first step involved the identification of the main binding modes with PELE, which was performed for both protonation forms of SA (calculations were made at pH 5, Fig. 4). Then, SA oxidation was estimated through spin densities from QM/MM simulations (Table 3). PELE results indicate that protonated SA (SAH) binds with higher affinity in the vicinity of the T1 site in 3A4 laccase (Fig. 4A): inspection of structures with interaction energy below −100 kcal mol^{-1} confirms that 19 out of 20 SAH binding modes were found inside the T1 cavity (hereafter named site 1, Fig. 5A). At this site the substrate's carboxylic acid is interacting with P393 and N207, while the phenolic group is surrounded by A162, P163 and the side chain of S264. In this site we find an average substrate spin density of 88%. For deprotonated SA (SA^-), however, site 1 is less populated and a second minimum appears (Fig. 4B). Site 1 seen in Fig. 5B shows the substrate in a different orientation and further away from the metal center due to the favorable interaction between the negatively charged carboxylate group and the backbone of G391 and F392 and the hydroxyl group of S387. Nevertheless, site 1 shows an average 87% spin density (although only one third of the analyzed structures correspond to this site), while the second minimum is less reactive (61% spin density, Table 3). Furthermore, SA^- is on average less protected from solvent than SAH, as seen by the higher solvent-accessible surface area (SASA) at the best interaction energies (Fig. S5†). All these data indicate the preference of 3A4 laccase for SAH oxidation over SA^-.

In C14F12, SAH presents two degenerate minima at 7 Å and at 12 Å (Fig. 4C); both sites are also present in 3A4, although C14F12 has an increased population at the second minimum. The spin density for SAH at site 1 (85%) is similar to that of 3A4, but the second minimum shows reduced spin density (40%, Table 3). Conversely, SA^- binds mainly in site 1 (Fig. 4D). As in the case of 3A4, the substrate's carboxylate group interacts with the backbone of G391 and N392 and S387's side chain. However, mutation F392N causes the rotation of the backbone, creating a favorable binding site for the negatively charged substrate with the N392 side chain. Despite the anchored carboxylate group, the substrate's phenolic group shows two main orientations with different oxidation rates: inside the T1 Cu site, which is more frequent, interacting with the P163 backbone and near D205 (93% spin density, Fig. 6A) or pointing directly to the solvent (48% spin

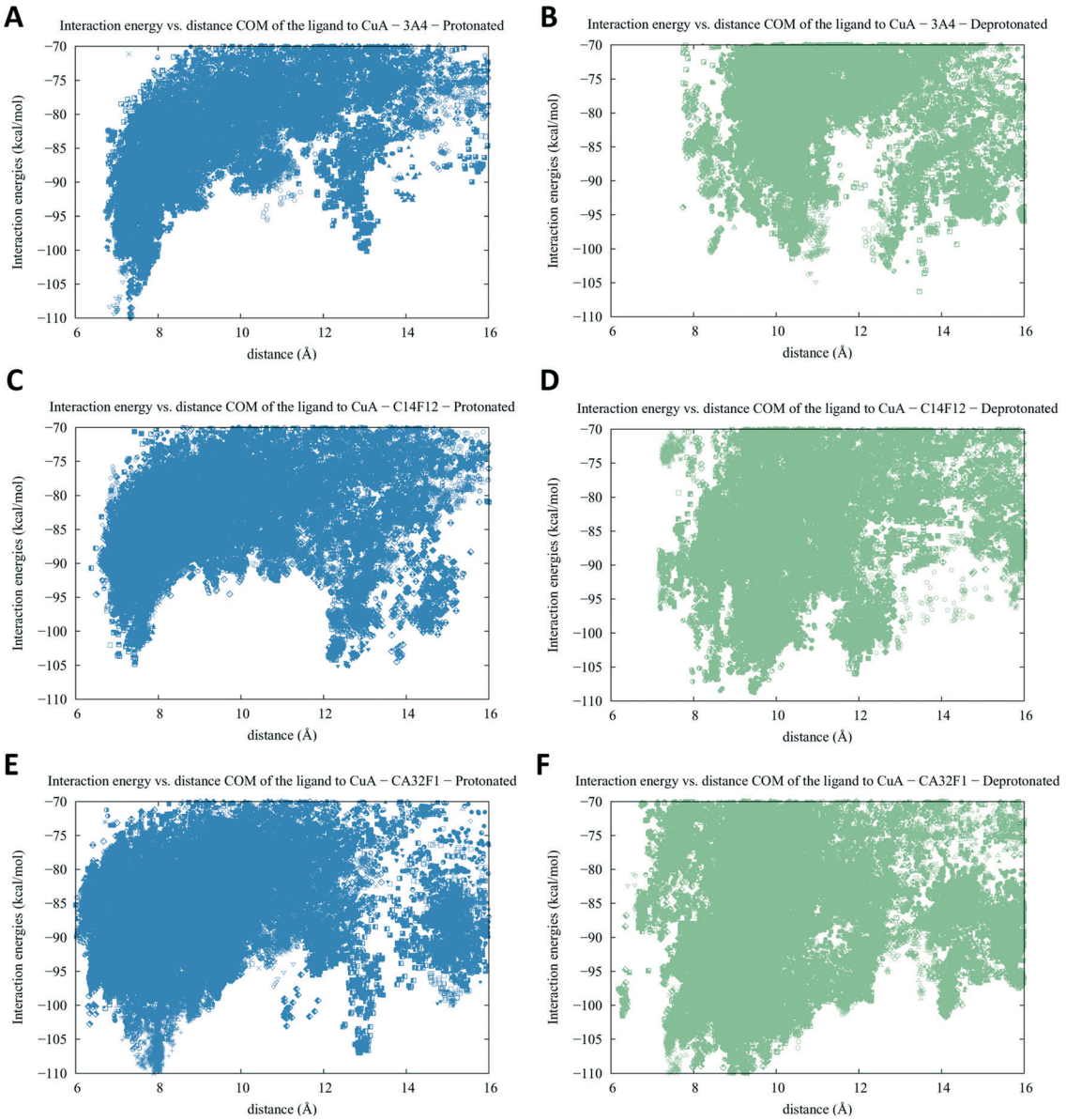

Fig. 4 Interaction energy *versus* the T1 copper–substrate (center of mass) distance for 3A4 (A, B), C14F12 (C, D) and CA32F1 (E, F) variants; conformational search of SAH (A, C, E) and SA^- (B, D, F).

density, Fig. 6B). These results suggest that the shifted pH activity profile and the improved activity seen at pH 5 for C14F12 (k_{cat} = 251 s^{-1}) relative to 3A4 (k_{cat} = 156 s^{-1}) could be mainly due to improved oxidation of SA^-, which is more

Table 3 Average spin density (%) on the substrate at site 1 for the different QM/MM calculations. Standard deviations are indicated as well as the proportion of structures corresponding to site 1 of all those evaluated

	3A4		C14F12		CA32F1	
	Poses	Spin density (%)	Poses	Spin density (%)	Poses	Spin density (%)
SAH	0.95	88 ± 6	0.65	85 ± 5	0.89	83 ± 20
SA^-	0.33	87 ± 8	0.75	82 ± 10	0.95	86 ± 9
DAD	0.45	80 ± 8	0.69	88 ± 6	0.29	100 ± 1

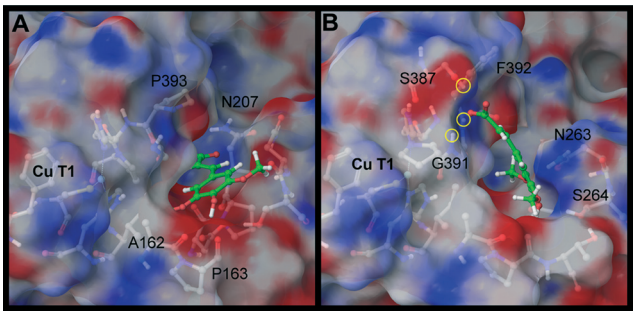

Fig. 5 Representative binding modes for SA in 3A4. (A) includes the most reactive mode for SAH while (B) corresponds to SA^-. The main residues participating in the backbone amine site are identified with yellow circles.

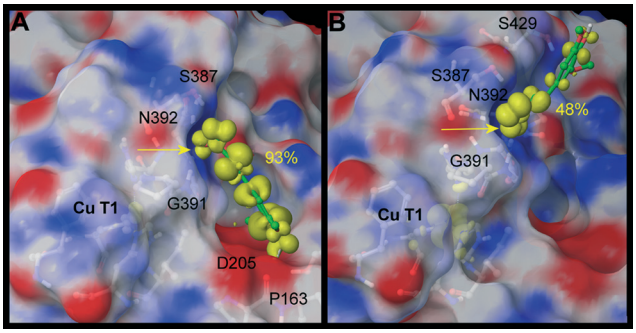

Fig. 6 Representative binding modes for SA^- with C14F12 protein. (A) includes the most reactive mode (in yellow, the spin density isosurface on the substrate) and (B) corresponds to a less active orientation with the carbonyl group exposed to the solvent. Arrows locate the carboxylate anchor point.

abundant at this pH than at pH 3. In agreement with this is the fact that the k_{cat} values for 3A4 and C14F12 at pH 3 are very similar (313 and 338 s^{-1}, respectively).

MD simulation performed for CA32F1 laccase (Fig. S6 and S7†) shows that R162 is mostly interacting with E164, but in ~25% of the time R162 is also interacting with D205, as a result of the flexibility observed in the loop hosting R162 and E164. Following MD relaxation, PELE simulations further confirmed the existence of these two conformations. For SAH, site 1 is highly populated (Fig. 4E) and two possible binding modes are observed: i) one very reactive (99% spin density) due to the favorable stacking of substrate between the two negatively charged residues (D205 and E164, Fig. 7A) and ii) a less reactive one (75%) due to simultaneous interaction of D205, R162 and E164 (Fig. 7B). In the case of SA^-, again it is found almost exclusively in site 1 (Fig. 4F). In fact, 19 out of 20 structures were in this site with an average 86% spin density (Table 3). SA^- is anchored by G391, F392 and S387, similar to the most reactive binding mode found in C14F12, although not as well positioned due to the presence of the large side chain of R162. This indicates that the relative orientation of the side chains from R162, E164 and D205

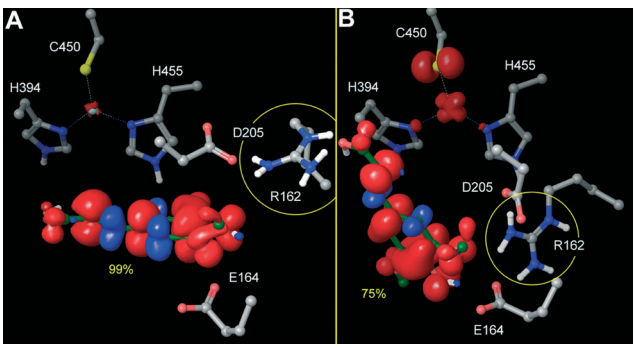

Fig. 7 Representative protein–substrate complexes for CA32F1 and SAH. Spin density isosurfaces are shown in red and blue. (A) Example of a conformation where the substrate is stacked between the two acids; (B) shows a less favorable oxidation position with simultaneous D205–R162–E164 interaction.

affects the oxidation of the substrate. In fact, an arginine residue in the substrate binding pocket of CotA laccase has recently been described to be crucial for SA oxidation. The crystal structure reveals that its side chain rotates 10° upon SA binding, sandwiching the substrate between itself and the T1 Cu site.[55] Finally, the SASA analysis shows a more buried interaction of the substrate at the T1 copper site in CA32F1, particularly in the case of SAH (Fig. S5E and F†).

We have also investigated the effect of lowering the pH to 3 but predictions indicate that only CA32F1 could undergo changes in the binding pocket. With an estimated pK_a of 3.8, D205 could be protonated, so calculations were repeated with SAH and both protonation states for D205. In this case PELE results indicate that SAH also binds in site 1, but the orientation of the ligand is different from that observed when D205 is not protonated. Also, low spin densities (18–65%) are obtained when using the neutral form of D205, while values up to 100% are obtained for deprotonated D205. Hence, the improved catalytic efficiency of CA32F1 on SA at pH 3 can be attributed to the favorable oxidation of SAH (the dominant species at this pH) and not to changes occurring in the protein. Although the estimated pK_a shows that catalytic D205 coexists in protonated and deprotonated forms in this variant at pH 3, binding SAH would displace the equilibrium, shifting the D205 population towards the carboxylate form and allowing proton transfer from the substrate to the protein. Indeed, mutation of the equivalent residues for non-acidic amino acids in laccases from *T. versicolor* (D206A) and *Melanocarpus albomyces* (E235T) severely affected the oxidation of phenolic substrates, especially at acidic pH.[25,46,56]

Taking all these results into account, we can conclude that the increased turnover rates for SA at pH 5 are caused by the enhanced oxidation of SA^- due to the anchoring of the substrate's carboxylate group by mutation F392N. However, in the C14F12 variant this is at the expense of SAH oxidation. On the other hand, CA32F1 is very active on both protonation forms of SA, presenting also increased k_{cat} at pH 3 with respect to parent 3A4, although the relative position of the new acid–basic pair formed by R162 and E164 is determinant for efficient binding of the substrate.

Finally, simulations were also performed for DAD with the three proteins. They all presented more or less similar binding in site 1, although it's worth noting that in the CA32F1 variant the interaction between R162 and E164 is observed in several structures, blocking the entrance of DAD into the substrate pocket. Overall, QM/MM results (Table 3) are in agreement with the similar turnover rates obtained for DAD with the three laccases. The CA32F1 variant showed up to 100% spin density, but due to the low proportion of site 1 structures used, these results were inconclusive.

Oxidation of related syringyl-type phenols

We also evaluated the oxidation of other syringyl-type phenols (with two *o*-methoxyl substituents) by the three laccase variants, determining their kinetic constants towards methyl

Table 4 Kinetic constants for the oxidation of MS, DMP, SyA and MSy (pH 5)

Substrate		3A4	C14F12	CA32F1
MS	k_{cat} (s^{-1})	195 ± 5	250 ± 5	309 ± 7
	K_m (μM)	12.0 ± 1.1	16.0 ± 0.9	18.6 ± 1.2
	k_{cat}/K_m	16 ± 2	15.6 ± 1.2	16.6 ± 1.4
DMP	k_{cat} (s^{-1})	90 ± 1	131 ± 3	128 ± 2
	K_m (μM)	46 ± 2	320 ± 30	191.7 ± 1.1
	k_{cat}/K_m	2.0 ± 0.1	0.41 ± 0.05	0.668 ± 0.014
SyA	k_{cat} (s^{-1})	57 ± 1	71 ± 3	63 ± 1
	K_m (μM)	32.9 ± 2.5	189 ± 4	102 ± 5
	k_{cat}/K_m	1.7 ± 0.2	0.38 ± 0.02	0.61 ± 0.04
MSy	k_{cat} (s^{-1})	71 ± 2	66 ± 1	68 ± 1
	K_m (μM)	132 ± 14	890 ± 30	710 ± 30
	k_{cat}/K_m	0.54 ± 0.07	0.082 ± 0.004	0.096 ± 0.005

sinapate (MS), 2,6-dimethoxyphenol (DMP), syringic acid (SyA) and methyl syringate (MSy) at pH 5 (Table 4). These substrates, differing in the presence or absence of a carboxylic group and the length of the aliphatic side chain, would help us understand the importance of the new binding mode created by mutation F392N, which was solely responsible for the increased k_{cat} obtained towards SA in the first generation. The kinetic constants obtained for MS were similar to those of SA, with a 1.5-fold increase in k_{cat} and also in K_m, resulting in a similar efficiency among the different laccase variants. However, catalytic efficiencies for DMP, SyA and MSy were severely impaired due to similar k_{cat} values and an important increase in K_m values (3- to 7-fold with respect to the parent type). Additional simulations were performed to elucidate the improved oxidation of MS in C14F12. The minimum with highest spin density (ranging from 65% to 73%) for parent 3A4 is very different from that found in variant C14F12 (with spin density ranging from 78% to 90%, Fig. S9†). In fact, C14F12 minima resemble the previously seen site 1 for SA^-, with a favorable interaction between MS's carbonyl and the backbone of N392 and, more importantly, with the phenolic group well positioned for proton abstraction at D205. This is not seen in 3A4, where the substrate is in a different orientation, probably due to steric hindrance of F392 on the extra methyl group. These results suggest that the opening of the T1 cavity by the replacement of F392 by N could be mainly responsible for the increased activity towards MS in C14F12, contributing also to the enhancement of SA oxidation. On the other hand, the lower catalytic efficiencies towards DMP, SyA and MSy shown by ISM variants suggest that the length of the side chain present in SA and MS could also be an important factor for favorable substrate binding in the engineered variants, providing better interaction between the phenolic group and D205. Indeed, in a related work we evaluated the oxidation of a battery of lignin-derived phenols by selected laccase mutants from libraries A, B and C enumerated in Table S2.† In this screening we observed a more pronounced increase in activity for mutants with F392N mutation towards SA, MS, ferulic acid and methyl ferulate than towards SyA, MSy, vanillic acid and methyl vanillate, respectively, which differ in the presence or absence of the propenyl chain.[57]

Conclusions

Combinatorial saturation mutagenesis on the substrate binding pocket together with experimental characterization and computational analysis of the resulting variants provided valuable information on the structural determinants for the oxidation of sinapic acid and related phenols by laccase. The results obtained put in evidence that the diversity of substrate binding pockets of fungal laccases in nature stands for the varied oxidation capabilities found in these generalist enzymes even if they hold similar redox potentials. Although the latter will be limiting the electron transfer between the substrate and the T1 copper, the binding event plays a crucial role in the overall rate of the reaction by creating an appropriate environment and substrate positioning that allows the oxidation to proceed. Concerning the engineering of laccases by rational design, it is shown that educated guesses may be misleading even for assessing the effect of a single mutation. The oxidation of each ligand is a unique combination of many factors. Thus, to engineer the enzyme, it is decisive to define the particular substrate and conditions for which the biocatalyst will be used, stressing the usefulness of atomic simulations in unveiling the molecular determinants for the efficient oxidation of a target molecule.

Abbreviations

ABTS	2,2′-Azino-bis(3-ethylbenzothiazoline-6-sulfonic acid)
CDS	Coding DNA sequence
CSM	Combinatorial saturation mutagenesis
DAD	Dehydrodisinapic acid dilactone
DMP	2,6-Dimethoxyphenol
HRPL	High redox potential laccase
ISM	Iterative saturation mutagenesis
IVOE	*In vivo* overlap extension
MD	Molecular dynamics
MS	Methyl sinapate
MSy	Methyl syringate
PELE	Protein energy landscape exploration
QM/MM	Quantum mechanics/molecular mechanics
SA	Sinapic acid
SAH	Protonated SA
SA^-	Deprotonated SA
SASA	Solvent-accessible surface area
SyA	Syringic acid
TAI	Total activity increase

Acknowledgements

This work was funded by INDOX (KBBE-2013-7-613549) European project and NOESIS (BIO2014-56388-R) and CTQ2013-48287-R Spanish National Projects. I. P. and G. S. acknowledge the Spanish Research Council (CSIC) and MINECO for their respective predoctoral fellowships.

References

1 S. Camarero, D. Ibarra, M. J. Martinez and A. T. Martinez, *Appl. Environ. Microbiol.*, 2005, **71**, 1775–1784.
2 S. Camarero, A. I. Cañas, P. Nousiainen, E. Record, A. Lomascolo, M. J. Martínez and A. T. Martinez, *Environ. Sci. Technol.*, 2008, **42**, 6703–6709.
3 A. I. Cañas and S. Camarero, *Biotechnol. Adv.*, 2010, **28**, 694–705.
4 S. Camarero, M. J. Martínez and A. T. Martínez, *Biofuels, Bioprod. Biorefin.*, 2014, **8**, 615–625.
5 I. Pardo and S. Camarero, *Cell. Mol. Life Sci.*, 2015, **72**, 897–910.
6 D. Maté, C. García-Burgos, E. García-Ruiz, A. O. Ballesteros, S. Camarero and M. Alcalde, *Chem. Biol.*, 2010, **17**, 1030–1041.
7 S. Camarero, I. Pardo, A. I. Cañas, P. Molina, E. Record, A. T. Martinez, M. J. Martinez and M. Alcalde, *Appl. Environ. Microbiol.*, 2012, **78**, 1370–1384.
8 I. Pardo, A. I. Vicente, D. M. Mate, M. Alcalde and S. Camarero, *Biotechnol. Bioeng.*, 2012, **109**, 2978–2986.
9 M. Bunzel, J. Ralph, H. Kim, F. Lu, S. A. Ralph, J. M. Marita, R. D. Hatfield and H. Steinhart, *J. Agric. Food Chem.*, 2003, **51**, 1427–1434.
10 N. Nićiforović and H. Abramovič, *Compr. Rev. Food Sci. Food Saf.*, 2014, **13**, 34–51.
11 A. Gaspar, M. Martins, P. Silva, E. M. Garrido, J. Garrido, O. Firuzi, R. Miri, L. Saso and F. Borges, *J. Agric. Food Chem.*, 2010, **58**, 11273–11280.
12 L. G. Landry, C. C. S. Chapple and R. L. Last, *Plant Physiol.*, 1995, **109**, 1159–1166.
13 M. Jurado, A. Prieto, Á. Martínez-Alcalá, Á. T. Martínez and M. J. Martínez, *Bioresour. Technol.*, 2009, **100**, 6378–6384.
14 A. D. Moreno, D. Ibarra, J. L. Fernández and M. Ballesteros, *Bioresour. Technol.*, 2012, **106**, 101–109.
15 A. D. Moreno, E. Tomás-Pejó, D. Ibarra, M. Ballesteros and L. Olsson, *Biotechnol. Biofuels*, 2013, **6**, 160.
16 M. T. Reetz and J. D. Carballeira, *Nat. Protoc.*, 2007, **2**, 891–903.
17 C. Galli, P. Gentili, C. Jolivalt, C. Madzak and R. Vadalà, *Appl. Microbiol. Biotechnol.*, 2011, **91**, 123–131.
18 M. D. Toscano, L. De Maria, S. Lobedanz and L. H. Østergaard, *ChemBioChem*, 2013, **14**, 1209–1211.
19 N. Gupta, F. S. Lee and E. T. Farinas, *J. Mol. Catal. B: Enzym.*, 2010, **62**, 230–234.
20 C. Notredame, D. G. Higgins and J. Heringa, *J. Mol. Biol.*, 2000, **302**, 205–217.
21 G. E. Crooks, G. Hon, J.-M. Chandonia and S. E. Brenner, *Genome Res.*, 2004, **14**, 1188–1190.
22 M. Alcalde, in *Methods in Molecular Biology*, ed. J. Braman, 2010, vol. 634, pp. 3–14.
23 I. Pardo, X. Chanagá, A. I. Vicente, M. Alcalde and S. Camarero, *BMC Biotechnol.*, 2013, **13**, 90.
24 E. García-Ruiz, D. Maté, A. Ballesteros, A. T. Martinez and M. Alcalde, *Microb. Cell Fact.*, 2010, **9**, 17.
25 C. Galli, C. Madzak, R. Vadalà, C. Jolivalt and P. Gentili, *ChemBioChem*, 2013, **14**, 2500–2505.
26 F. Xu, W. Shin, S. H. Brown, J. A. Wahleithner, U. M. Sundaram and E. I. Solomon, Biochim, *Biochim. Biophys. Acta, Protein Struct. Mol. Enzymol.*, 1996, **1292**, 303–311.
27 G. J. Fan, X. L. Jin, Y. P. Qian, Q. Wang, R. T. Yang, F. Dai, J. J. Tang, Y. J. Shang, L. X. Cheng, J. Yang and B. Zhou, *Chem. – Eur. J.*, 2009, **15**, 12889–12899.
28 F. Lu and J. Ralph, *Org. Biomol. Chem.*, 2008, **6**, 3681–3694.
29 K. Freudenberg and H. Schraube, *Chem. Ber.*, 1955, **88**, 16–23.
30 D. Shivakumar, J. Williams, Y. Wu, W. Damm, J. Shelley and W. Sherman, *J. Chem. Theory Comput.*, 2010, **6**, 1509–1519.
31 G. Madhavi Sastry, M. Adzhigirey, T. Day, R. Annabhimoju and W. Sherman, *J. Comput.-Aided Mol. Des.*, 2013, **27**, 221–234.
32 M. H. M. Olsson, C. R. Søndergaard, M. Rostkowski and J. H. Jensen, *J. Chem. Theory Comput.*, 2011, **7**, 525–537.
33 R. Anandakrishnan, B. Aguilar and A. V. Onufriev, *Nucleic Acids Res.*, 2012, **40**, 537–541.
34 M. Ragnar, C. T. Lindgren and N.-O. Nilvebrant, *J. Wood Chem. Technol.*, 2000, **20**, 277–305.
35 A. D. Bochevarov, E. Harder, T. F. Hughes, J. R. Greenwood, D. A. Braden, D. M. Philipp, D. Rinaldo, M. D. Halls, J. Zhang and R. A. Friesner, *Int. J. Quantum Chem.*, 2013, **113**, 2110–2142.
36 K. W. Borrelli, A. Vitalis, R. Alcantara and V. Guallar, *J. Chem. Theory Comput.*, 2005, **1**, 1304–1311.
37 A. R. Atilgan, S. R. Durell, R. L. Jernigan, M. C. Demirel, O. Keskin and I. Bahar, *Biophys. J.*, 2001, **80**, 505–515.
38 G. A. Kaminski, R. A. Friesner, J. Tirado-Rives and W. L. Jorgensen, *J. Phys. Chem. B*, 2001, **105**, 6474–6487.
39 D. Bashford and D. A. Case, *Annu. Rev. Phys. Chem.*, 2000, **51**, 129–152.
40 R. B. Murphy, D. M. Philipp and R. A. Friesner, *J. Comput. Chem.*, 2000, **21**, 1442–1457.
41 R. S. Mulliken, *J. Chem. Phys.*, 1955, **23**, 1833.
42 P. J. Hay and W. R. Wadt, *J. Chem. Phys.*, 1985, **82**, 270.
43 W. J. Hehre, R. Ditchfield and J. A. Pople, *J. Chem. Phys.*, 1972, **56**, 2257–2261.
44 P. Alvira, A. D. Moreno, D. Ibarra, F. Sáez and M. Ballesteros, *Biotechnol. Prog.*, 2013, **29**, 74–82.
45 T. Bertrand, C. Jolivalt, P. Briozzo, E. Caminade, N. Joly, C. Madzak and C. Mougin, *Biochemistry*, 2002, **41**, 7325–7333.
46 J. P. Kallio, S. Auer, J. Jänis, M. Andberg, K. Kruus, J. Rouvinen, A. Koivula and N. Hakulinen, *J. Mol. Biol.*, 2009, **392**, 895–909.
47 K. Koschorreck, S. M. Richter, A. Swierczek, U. Beifuss, R. D. Schmid and V. B. Urlacher, *Arch. Biochem. Biophys.*, 2008, **474**, 213–219.
48 T. Bulter, M. Alcalde, V. Sieber, P. Meinhold, C. Schlachtbauer and F. H. Arnold, *Appl. Environ. Microbiol.*, 2003, **69**, 987–995.
49 G. Festa, F. Autore, F. Fraternali, P. Giardina and G. Sannia, *Proteins*, 2008, 25–34.
50 P. Torres-Salas, D. M. Mate, I. Ghazi, F. J. Plou, A. O. Ballesteros and M. Alcalde, *ChemBioChem*, 2013, **14**, 934–937.
51 K. Lacki and Z. Duvnjak, *Biotechnol. Bioeng.*, 1998, **57**, 694–703.

52 M. A. Tadesse, A. D'Annibale, C. Galli, P. Gentili and F. Sergi, *Org. Biomol. Chem.*, 2008, **6**, 868.
53 P. Muller, *Pure Appl. Chem.*, 1994, **66**, 1077–1184.
54 E. Monza, M. F. Lucas, S. Camarero, L. C. Alejaldre, A. T. Martínez and V. Guallar, *J. Phys. Chem. Lett.*, 2015, **6**, 1447–1453.
55 T. Xie, Z. Liu, Q. Liu and G. Wang, *J. Struct. Biol.*, 2015, **190**, 155–161.
56 C. Madzak, M. C. Mimmi, E. Caminade, A. Brault, S. Baumberger, P. Briozzo, C. Mougin and C. Jolivalt, *Protein Eng., Des. Sel.*, 2006, **19**, 77–84.
57 I. Pardo and S. Camarero, *Molecules*, 2015, **20**, 15929–15943.